VISCID-INVISCID INTERACTION ON AIRFOILS USING EULER AND INVERSE BOUNDARY-LAYER EQUATIONS

By

D. Whitfield
Mississippi State University

A. Jameson
Princeton University

Wolfgang Schmidt
Dornier GmBh, West Germany

US-German Data Exchange Meeting
DFVLR-AAVA
Gottingen, 1981

VISCID - INVISCID INTERACTION ON AIRFOILS USING EULER AND INVERSE BOUNDARY-LAYER EQUATIONS

David Whitfield, Professor
Department of Aerospace Engineering
Mississippi State University
Mississippi State, MS 39762
and
Antony Jameson, Professor
Department of Mechanical and Aerospace Engineering
Princeton University
Princeton, NJ 08544
and
Wolfgang Schmidt
Dornier GMBH
D-7990 Friedrichshafen
West Germany

ABSTRACT

An Euler equation code is coupled with a boundary-layer code for calculating viscid-inviscid interaction on airfoils. The Euler equation code is a new finite volume three-step scheme that is stable for Courant numbers up to two. The boundary-layer code is an inverse mean-flow kinetic energy integral method. Viscid-inviscid coupling is achieved using the surface source method. Calculations were made for transonic flow over an airfoil and compared with experimental surface pressure and boundary-layer data.

1. INTRODUCTION

Methods available for calculating transonic viscid-inviscid interacting flow over airfoils are either Navier-Stokes methods or inviscid methods coupled with boundary-layer solutions. Whereas the Navier-Stokes equations properly describe interacting flow, these equations are presently restricted from routine use because of computer requirements. Inviscid flow boundary-layer coupling methods on the other hand require less computer resources, but these methods have been developed for irrotational inviscid flow and usually attached boundary layers. Recent reviews of viscid-inviscid coupling methods by Lock[1] and Melnik[2] are available, hence a review of previous work is not included here. The purpose of this paper is to report on computations of transonic viscid-inviscid interacting flow on airfoils which are based on coupling an Euler equation code to allow for rotational inviscid flow, with an inverse boundary-layer code to allow for attached or separated flow.

Lock[1] points out that the use of potential flow equations introduces a source of error and uncertainty because the flow is assumed to be everywhere irrotational and isentropic. Lock[1] illustrates that the pressure rise for an isentropic shock is greater than that for a true shock, with the difference becoming appreciable for local Mach numbers greater than 1.2. Therefore, because many flows of practical interest have local Mach numbers greater than 1.2, there is need of a method for calculating viscid-inviscid interacting flow without the restriction of irrotational, isentropic

inviscid flow.

Lock[1] also points out that attached flow boundary-layer methods require an artificial safety valve to prevent the breakdown of the method past separation. This is particularly a problem in passing through a shock wave and at the trailing edge of an airfoil. Moreover, this problem can be compounded in the early iteration cycles where the shocks may be strong even if the final solution contains no regions of separated flow. It is assumed that these artificial fixes do not significantly influence the final solution.[1] This problem is overcome in the present method by using an inverse boundary-layer method that permits regions of separated flow during the iteration cycles and/or in the final converged solution.

The method used for solving the Euler equations is a new method due to Jameson, Rizzi, Schmidt, and Turkel.[3] The inverse boundary-layer method is that described in Ref. 4. The Euler equation method is discussed first, followed by a description of the inverse boundary-layer method. The method used to couple the viscid-inviscid solutions is then described, followed by computed results for supercritical flow over an airfoil for which experimental surface pressure and boundary-layer data are available.

II. EULER EQUATION METHOD

The numerical method used to solve the Euler equations is described in Ref. 3. The method is a new unsplit, three-step (one predictor and two correctors), finite volume scheme. The scheme is second order accurate and a Fourier analysis indicates the scheme is stable for the one dimensional initial value problem for Courant numbers up to 2. Steady flow calculations are further accelerated by using a variable time step determined at each grid point by the local Courant number. The energy equation is not solved, rather the steady state condition of constant total enthalpy is used to determine the pressure. The basic time stepping scheme is followed by a filter at each time step which introduces an effective artificial viscosity. This filter helps stabilize the scheme for flows with shocks such that the expected limiting values of Courant number were used throughout the grid in the present calculations.

This Euler equation code is operational on the CRAY-1 and the CYBER 203 computers. However, no significant optimizations have yet been performed to fully utilize either machine, hence current computation times represent an upper bound and mean very little. For a 121 x 30 mesh, one cycle requires about 0.15 seconds on the CRAY-1 and the CYBER 203 requires about twice this much time. Reasonably converged solutions require 1000 cycles, although good engineering answers are obtained in 500 to 800 cycles.

III. INVERSE BOUNDARY-LAYER METHOD

The singularity associated with boundary-layer computations at separation is avoided by using an inverse boundary-layer calculation method. By specifying, for example, the displacement thickness distribution instead of the pressure distribution (a so-called inverse method) this singularity is removed[5] and boundary-layer computations can proceed throughout separated regions. The inverse method used here is the mean-flow kinetic energy integral method described in Ref. 4. This method is based on turbulent boundary-layer velocity profiles that describe separated or attached flow.

The same calculation scheme is used whether the flow is attached or separated and hence no switching or artificial fix is required for points near separation. The dissipation integral is evaluated at each streamwise location using the velocity profiles and the Cebeci-Smith algebraic eddy viscosity model.[6]

In an inverse boundary-layer method, pressure is a dependent variable, and in the particular inverse method used here the displacement thickness (δ^*) distribution is specified. The method used to provide a rational, a priori, specification of the δ^* distribution is the method of Carter.[7] Carter's method can be written as

$$\delta^{*(m+1)} = \delta^{*(m)} + \omega\delta^{*(m)}\left(\frac{u_{e,v}}{|\vec{q}|_{w,i}} - 1\right) \tag{1}$$

where $\delta^{*(m+1)}$ is the new displacement thickness at a streamwise location, $\delta^{*(m)}$ is the displacement thickness from the previous iteration, $u_{e,v}$ is the local velocity at the edge of the boundary layer obtained from the last boundary-layer solution, $|\vec{q}|_{w,i}$ is the magnitude of the local velocity vector obtained from the last Euler equation solution, and ω is the relaxation parameter.

Figure 1 illustrates that Eq. (1) can also be used with an inverse method to solve a conventional attached flow boundary-layer problem (albeit an increasingly adverse pressure gradient flow) with known pressure distribution. For such a problem, the known pressure distribution is used to determine the velocity distribution which corresponds to $|\vec{q}|_{w,i}$ in Eq. (1). In this case the term $|\vec{q}|_{w,i}$ would, of course, remain fixed at each streamwise location and Eq. (1), with $u_{e,v}$ updated after each inverse boundary-layer solution, is used to obtain the converged δ^* distribution. Figure 1 illustrates that the inverse method, with Eq. (1) used for updating δ^*, provides essentially the same result as the direct method after about 4 iterations with $\omega = 2$ and the initial δ^* distribution being that for a flat plate. Therefore, although a direct method is faster than an inverse method for attached flow because iteration is not required, a direct method is not required.

IV. VISCID-INVISCID COUPLING

The method used to achieve viscid-inviscid coupling is the surface source model (or the method of equivalent sources of Lighthill[9]). This method has an advantage over the effective displacement surface approach in that a surface source mass flux is imposed as a boundary condition in the inviscid calculation at the physical body surface or in the wake, and hence mesh adjustment during the iteration process is not required. The surface source mass flux, $(\rho v)_n$, imposed at the physical surface is given by

$$(\rho v)_n = \frac{d(\rho_e u_e \delta^*)}{dx} \tag{2}$$

where $(\rho v)_n$ is the local mass flux normal to the surface. The right hand side of Eq. (2) is evaluated after each inverse boundary-layer solution to

determine $(\rho v)_n$ for subsequent inviscid calculations.

The viscid-inviscid interaction calculation scheme proceeds in the following steps.

1. The Euler equation solution is advanced 20 to 50 cycles with $(\rho v)_n \equiv 0$.
2. An inverse boundary-layer solution is obtained with $\delta^{*(1)}$ given by Eq. (1), where $\delta^{*(0)}$ is a flat plate distribution, $u_{e,v}$ is constant at the free-stream value (u_∞), and $|\vec{q}|_{w,i}$ is obtained from the last cycle of the Euler equation solution.
3. The Euler equation solution is advanced 20 to 50 cycles with $(\rho v)_n$ held fixed at the value given by Eq. (2).
4. An inverse boundary-layer solution is obtained with $\delta^{*(m+1)}$ given by Eq. (1).
5. Steps 3 and 4 are repeated until convergence on δ^* or c_p (surface pressure coefficient) is obtained.

The number of cycles the Euler equation solution is advanced in steps 1 and 3 depends upon the problem. For example, if strong shocks form in the early cycles of the Euler equation solution and if over relaxation is used, like $\omega = 2$, it can be advantageous to call the inverse boundary-layer solution after only a few cycles. It is possible to obtain a converged viscid-inviscid interaction solution in fewer cycles than required to obtain a converged inviscid solution due to a weaker shock resulting from the inclusion of viscous effects. However, most solutions presented were cycled 1.5 to 2 times the number of cycles required for a purely inviscid solution.

V. RESULTS

The experimental data of Cook, McDonald, and Firmin[10] include surface pressure and boundary-layer information for transonic flow about the RAE 2822 airfoil. Two sets of experimental data, denoted as Cases 6 and 9 in Ref. 10, are considered. Unfortunately these data, as all available transonic airfoil data, are not interference free. The values of Mach number and angle of attack corresponding to experimental (wind tunnel) conditions were

Case 6	Case 9
$M_\infty = 0.725$	$M_\infty = 0.730$
$\alpha = 2.92°$	$\alpha = 3.19°$

and the corrected Mach number and angle of attack values used for the present inviscid and viscid-inviscid interaction calculations were

Case 6	Case 9
$M_{\infty,corr} = 0.729$	$M_{\infty,corr} = 0.734$
$\alpha_{corr} = 2.44°$	$\alpha_{corr} = 2.67°$

The Reynolds number based on chord was 6.5×10^6 for both cases.

Comparisons of calculated and measured surface pressure data are given in Figs. 2 and 3. The Mach number correction of 0.004 was that used by Lock[1] to obtain agreement between calculated and measured lower surface pressure distributions using a potential flow code for the inviscid flow. However, note in Figs. 2 and 3 that the lower surface agreement obtained

here using this Mach number correction is not good. The corrected angle of attacks were determined by the information provided by Cook, McDonald, and Firmin.[10] The calculated shock location using the corrected angle of attack is close to the experimental shock location for Case 9 in Fig. 3, but the calculated shock location for Case 6 in Fig. 2 is about 3 percent chord forward of the experimental shock location. Adjustments in Mach number and angle of attack to match surface pressure distributions and hence lift coefficients were not made.

Comparisons of calculated and measured boundary-layer data are given in Figs. 4-6. The calculated boundary-layer displacement thickness (δ^*/c) and momentum thickness (θ/c) distributions are slightly above the experimental data over the aft portion of the airfoil for Case 6 in Fig. 4. However, the calculated shock location is slightly forward of the experimental shock location as mentioned above, which may contribute to this difference. The calculated c_f, δ^*/c, and θ/c distributions for the stronger shock case in Fig. 5 are in good agreement with the experimental data, even in the shock boundary-layer interaction region. A more detailed comparison of calculated and measured data throughout the shock region and at the trailing edge is given in Fig. 6 by boundary-layer velocity profile comparisons. The agreement between calculated and measured data in Fig. 6 is considered good. Calculated distributions of the source velocity, $(\rho v)_n$, are included in Figs. 4 and 5. This term becomes significant in, and downstream, of the shock with large positive values occurring in the shock region and at the trailing edge. The source velocity becomes negative in the wake and reaches a minimum just aft of the trailing edge.

VI. CONCLUDING REMARKS

The objectives of the present work were to develop a viscid-inviscid interaction calculation method for airfoils that was not restricted to irrotational, isentropic inviscid flow and which did not require artificial fixes in the boundary-layer calculation, particularly in the shock and trailing edge regions. High quality, interference free (or with all far field boundary conditions measured) experimental data are needed to verify such a method; unfortunately, such data are evidently not available. For the experimental data considered, the suggested Mach number corrections[1] and angle of attack corrections[10] did not bring the calculated results into agreement with the experimental data, particularly with regard to the lower surface pressure distributions. The calculated boundary-layer results were, however, in reasonable agreement with experimental data, particularly for the strong shock case (Case 9).

Preliminary, unpublished calculations performed by Drs. Benek and Jones at AEDC using various full potential and Euler equation calculation methods, indicate that potential and Euler equation solutions do not give the same lift and pitching moment coefficients for supercritical flow about an NACA 0012 airfoil. Therefore, the same Mach and angle of attack corrections may not apply to both potential and Euler equation calculation methods. Hence, a critical comparison between full potential and Euler equation solutions needs to be performed.

REFERENCES

1. Lock, R. L. "A Review of Methods for Predicting Viscous Effects on

Aerofoils and Wings at Transonic Speeds." AGARD-CPP-291, 1980.

2. Melnik, R. E. "Turbulent Interactions on Airfoils at Transonic Speeds - Recent Developments." AGARD-CPP-291, 1980.

3. Jameson, A., Rizzi, A., Schmidt, W., and Turkel, E. "Numerical Solutions of the Euler Equations by Finite Volume Methods Using Runge Kutta Time Stepping Schemes." AIAA Computational Fluid Dynamics Conference, June 1981.

4. Whitfield, D. L., Swafford, T. W., and Jacocks, J. L. "Calculation of Turbulent Boundary Layers with Separation, Reattachment, and Viscous-Inviscid Interaction." AIAA Paper No. 80-1439, July 1980.

5. Catherall, D. and Mangler, K. W. "The Integration of the Two-Dimensional Laminar Boundary-Layer Equations Past the Point of Vanishing Skin Friction." Journal of Fluid Mechanics, Vol. 26, Part 1, 163-183, 1966.

6. Cebeci, T. and Smith, A. M. O. Analysis of Turbulent Boundary Layers. Academic Press, New York, NY, 1974.

7. Carter, J. E. "A New Boundary-Layer Inviscid Iteration Technique for Separated Flow." AIAA Paper No. 79-1450, July 1979.

8. Samuel, A. E. and Joubert, P. N. "A Boundary Layer Developing in an Increasingly Adverse Pressure Gradient." Journal of Fluid Mechanics, Vol. 66, Part 3, 481-505, 1974.

9. Lighthill, M. J. "On Displacement Thickness." Journal of Fluid Mechanics, Vol. 4, Part 4, 383-392, 1958.

10. Cook, P. H., McDonald, M. A., and Firmin, M. C. P. "Airfoil RAE 2822 Pressure Distributions and Boundary Layer Measurements," in Experimental Data Base for Computer Program Assessment, AGARD-AR-138, 1979.

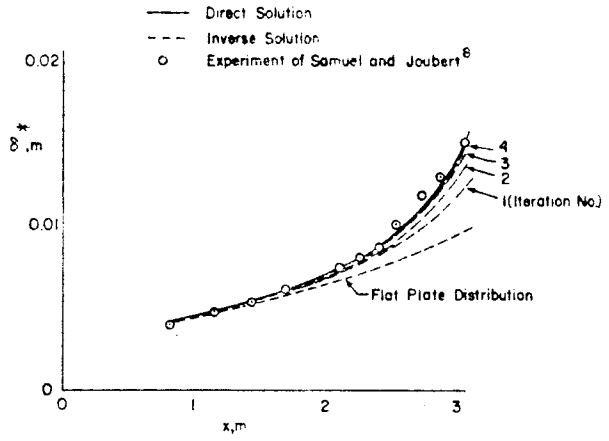

Fig. 1 Direct and Inverse Boundary-Layer Calculations of an Increasingly Adverse Pressure Gradient Flow

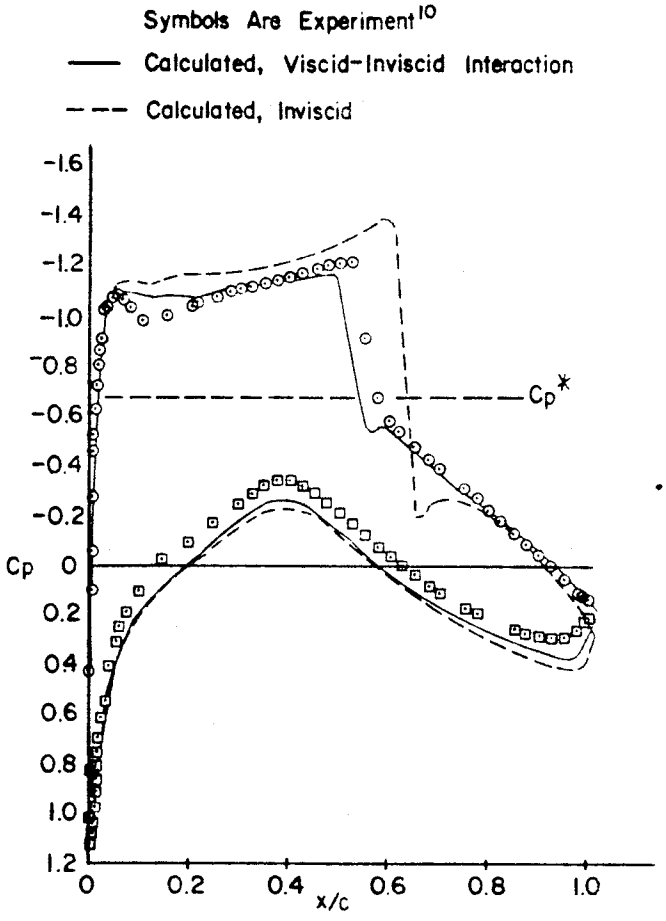

Fig. 2 Surface Pressures on the RAE 2822 Airfoil for Case 6

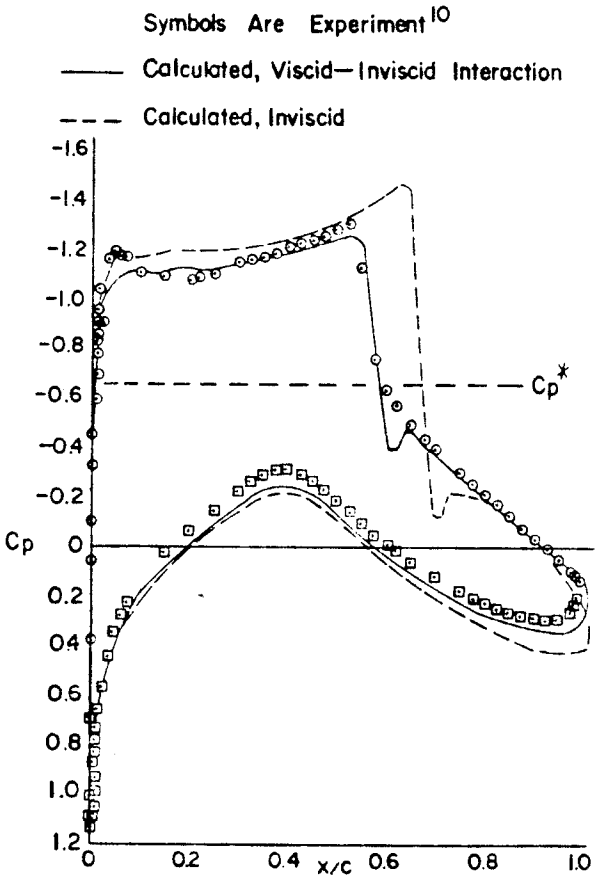

Fig. 3 Surface Pressures on the RAE 2822 Airfoil for Case 9

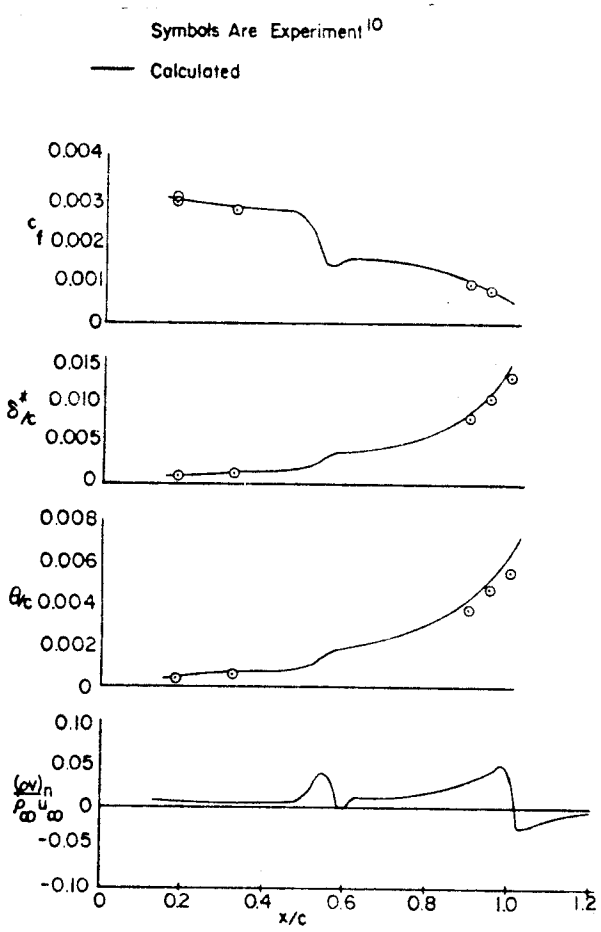

Fig. 4 Boundary-Layer Data on the RAE 2822 Airfoil Upper Surface for Case 6

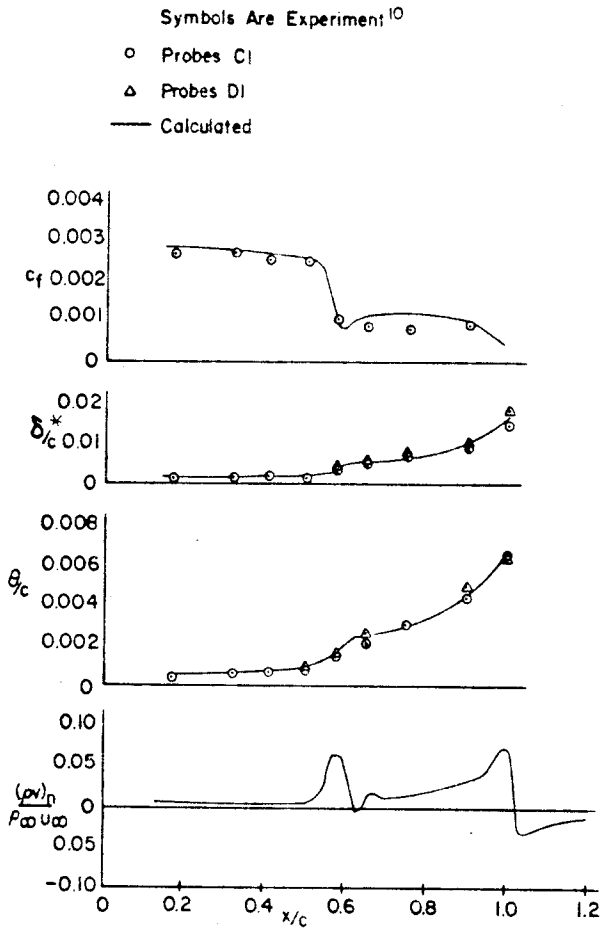

Fig. 5 Boundary-Layer Data on the RAE 2822 Airfoil Upper Surface for Case 9

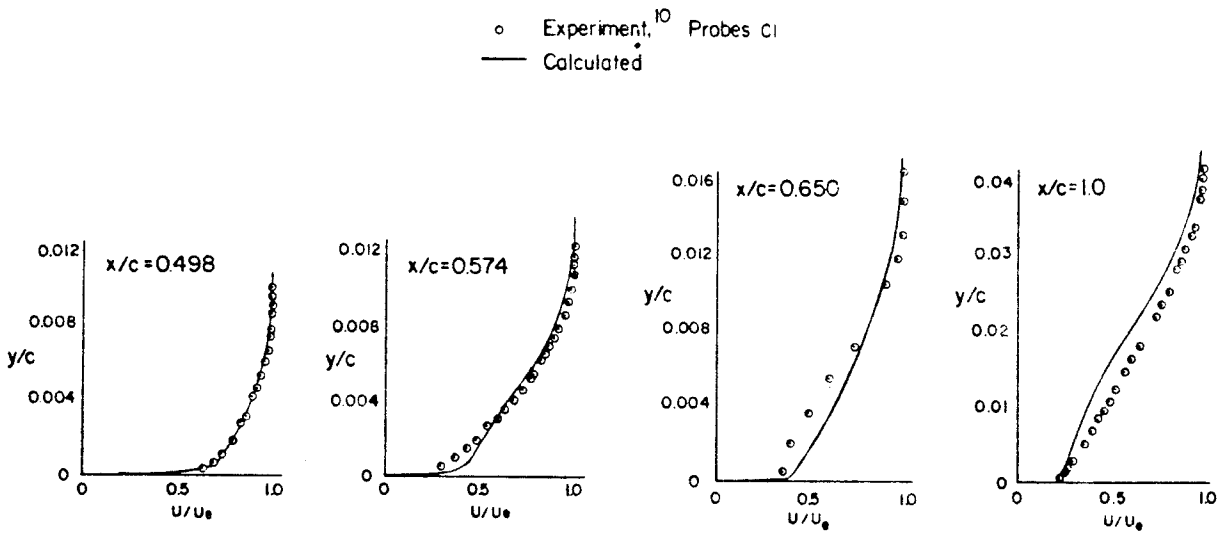

Fig. 6 Boundary-Layer Velocity Profiles on the RAE 2822 Airfoil Upper Surface for Case 9